Implications of magnetic-hysteresis-loop scaling in high-temperature superconductors

G. K. Perkins and L. F. Cohen
Centre for High Temperature Superconductivity, Blackett Laboratory, Imperial College, London SW7 2BZ, United Kingdom

A. A. Zhukov
Physics Department, Moscow State University, 117234 Moscow, Russia

A. D. Caplin
Centre for High Temperature Superconductivity, Blackett Laboratory, Imperial College, London SW7 2BZ, United Kingdom
(Received 26 September 1994)

We show how to incorporate the commonly observed scaling behavior of magnetic hysteresis loops $M(H)$ in $(R)Ba_2Cu_3O_{7-\delta}$ (R=rare earth) crystals into a systematic and straightforward analytical procedure that yields the key parameters associated with the vortex dynamics. If the effective barrier height for vortex motion is written in terms of a scale energy $U_0(B,T)$ and a scale current density $J_0(B,T)$, both the field and temperature dependences of these quantities can be found directly from the experimental data, without any deconvolution. The procedure is illustrated with the data on one specific sample of $TmBa_2Cu_3O_{7-\delta}$. Over a substantial region of the B-T plane, $J_0(B,T)$ is found to be $\propto B$ and essentially temperature independent; $U_0(B,T)$ is approximately $\propto 1/B$ and decreases steadily as T_c is approached. The competition between the field dependences of $J_0(B,T)$ and $U_0(B,T)$ gives rise to the ubiquitous "fishtail" in the magnetization loops.

I. INTRODUCTION

The irreversible magnetization loops [$M(H)$ loops] and the normalized flux creep rate S of high-temperature superconductors reflect the behavior of vortices in these materials. In principle, therefore, measurement and analysis of the $M(H)$ loops together with S, and their dependence on temperature and field, should allow the relevant physical quantities, particularly the effective pinning potential $U_{\rm eff}$, to be obtained as a function of field, temperature, and current density. In practice, there are sufficient unknowns that the problem has usually been phrased the other way around, and various theoretical models have been tested by attempting to fit the experimental data to them. This procedure is less than satisfactory, because it usually comes down to evaluating the reasonableness or otherwise of the fitting parameters, and also because it tends to obscure the physical significance of the features that are observed in the $M(H)$ loops themselves.

A prominent feature of the $M(H)$ loops of $YBa_2Cu_3O_{7-\delta}$ is the occurrence of an anomalous second peak or "fishtail." Its presence has led to the idea of scaling, in which a sequence of loops taken at widely different temperatures can be collapsed onto a single curve when M and H are appropriately normalized.[1–6] Recently, scaling behavior in the creep rate has also been reported.[6,7] Although there have been many attempts to evaluate $U_{\rm eff}(B,J,T)$ from such magnetization data (see Schnack *et al.*[8] and references therein), they have not previously incorporated this scaling into the strategy of the analysis.

The form of the $M(H)$ loop is governed by the behavior of the vortices in the presence of static and thermal disorder (assuming quantum effects are small), which are responsible for the phenomena of vortex pinning and vortex creep. Our motivation comes from the similarities we have seen, including the scaling of the $M(H)$ loops, in several well-oxygenated $(R)Ba_2Cu_3O_{7-\delta}$ crystals obtained from different sources.[6] Furthermore, as oxygen is removed from these crystals (which is probably associated with an increasingly anisotropic nature of the superconductivity), the magnetic behavior evolves in a systematic fashion.[9] Consequently, it is essential to have an unbiased analysis of the data, so that the changes in the vortex dynamics can be properly quantified.

The starting point is that magnetization measurements on superconductors, when properly conducted,[10] interrelate the four important physical variables: the temperature T, the magnetic induction B within the sample, the current density J, and the electric field E. Here we highlight the scaling of the $M(H)$ loops and go on to describe it analytically together with the creep rate S, but without imposing any specific model on the data. We proceed to find the implications of the scaling for the underlying physics and show how they can be compared with the predictions of theoretical models.

II. EXPERIMENTAL DATA SET

The approach to analyzing the $M(H)$ and S data that we develop here is a perfectly general one, requiring only that the $M(H)$ loops be observed to scale over a substantial range of magnetic field and temperature. The sample chosen to illustrate this approach is one of a set of microtwinned $TmBa_2Cu_3O_{7-\delta}$ crystals of slightly reduced oxygen content; the systematic investigation of the dependence of $M(H)$ and S with δ in these crystals is described in Ref. 9. This specific crystal has $\delta \approx 0.2$,

$T_c = 88$ K, and so is slightly underdoped, and also distinctly more anisotropic than fully oxygenated material.

Measurements were made on a commercial (Oxford Instruments) vibrating sample magnetometer of 8 T maximum applied field. The data set comprises $M(H)$ loops taken at temperatures T below about 80 K and at a number of different sweep rates H' of the applied magnetic field. Because our analysis essentially involves the small *differences* between loops taken at slightly different temperatures or at different sweep rates (Sec. III), the small magnetizations at temperatures above about 80 K give rise to rather noisy data, and they are excluded from the present discussion. In principle, there would be no difficulty in acquiring data much closer to T_c; it requires just that the signal-to-noise ratio be enhanced by the averaging of multiple $M(H)$ loops, and that would be time consuming.

Provided that the experimental conditions have been chosen carefully,[10] all the variables T, B, J, and E can be treated as if they are uniform through the sample, and also B set equal to $\mu_0 H$. The E field arises from induction, generated by the sweep of the applied magnetic field H (in relaxation measurements E comes from the time decay of the magnetization M). The current density $J(B)$ was calculated from the hysteresis width $\Delta M(B)$ using the Bean model.[11] The normalized creep rate $S(B)$ was obtained by the "dynamic" method,[12] in which ΔM is measured as a function of sweep rate H':

$$S = \left[\frac{\partial \ln \Delta M}{\partial \ln H'}\right]_{B,T} = \left[\frac{\partial \ln J}{\partial \ln E}\right]_{B,T}, \quad (1)$$

with $\mu_0 H'$ between 3 and 20 mT s^{-1}, generating electric fields in the range of $\sim 10^{-8}$–10^{-7} V m^{-1}.

III. EMPIRICAL SCALING OF $M(H)$ LOOPS

Figure 1 shows 24 separate $J(B)$ curves for the $TmBa_2Cu_3O_{7-\delta}$ crystal at six temperatures and four electric fields, plotted on double-logarithmic scales. These curves appear to translate to larger J and larger B as either the temperature T is decreased or as the magnetic field sweep rate H' that generates E is increased.

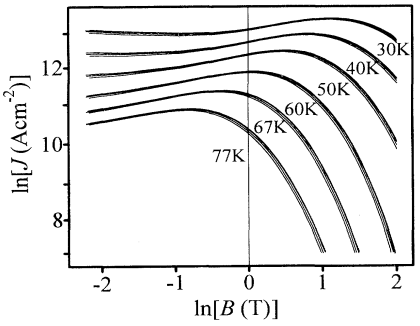

FIG. 1. Measured $J(B)$ for different temperatures and electric fields, obtained from magnetization loops on a $TmBa_2Cu_3O_{6.8}$ crystal and plotted on logarithmic scales. The closely spaced curves correspond to different sweep rates $\mu_0 H'$ in the range 3–20 mT/s, and so to different E, at fixed T.

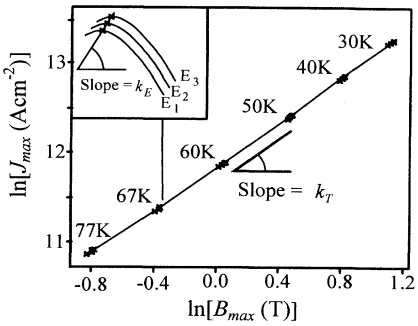

FIG. 2. Coordinates of the maximum (the fishtail peak) of each curve of Fig. 1. The closely spaced points mark variations in E at fixed T, and the associated schematic behavior of the $M(H)$ loops is indicated in the inset. Data points taken at constant T but different E fall on a curve of gradient k_E. Similarly, points at constant E but different T lie on a curve of gradient k_T. Both k_E and k_T are of the order of unity.

The fishtail peak provides a convenient fiducial point on the curves, and its coordinates (J_{max},B_{max}) are plotted directly in Fig. 2, so as to quantify the scaling. It is physically significant that in this sample, to a good approximation, changes in either T and E cause translations along the *same* straight line of gradient about unity. However, our analysis does not require that to be the case.

Figure 3 shows how the curves can be brought into near coincidence by scaling to the fishtail peak. The scaling between $J(B)$ of different E but at constant T is very precise, and the curves are indistinguishable by eye. Scaling between different temperatures is less perfect; both extrinsic and intrinsic factors may be relevant, for example, sample homogeneity and self-field effects at low B.[10] However, given that the unscaled curves span up to 2 orders of magnitude in J, the scaling is highly significant.

The central theme of this paper is that this scaling is an excellent first approximation to the measured magnetization and that therefore it should be incorporated at the outset into the description of the physical behavior.

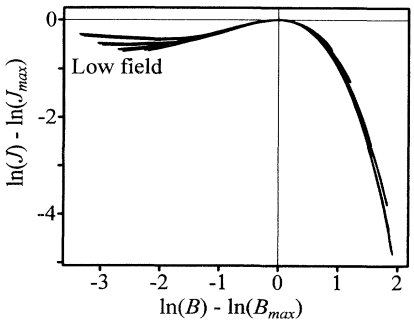

FIG. 3. The 24 curves of Fig. 1 rescaled so that their maxima coincide.

IV. ANALYTIC FORMULATION OF SCALING

Having established that the magnetization follows closely the scaling discussed in Sec. III, we now consider how to describe it analytically.

A. Ideal scaling

In order to develop the ideas, it is simplest to start with the idealized case in which the $M(H)$ loops scale perfectly at all magnetic fields and for all temperatures; we term this "ideal scaling." In Sec. IV B below, we then go on to discuss how the results may be applied to the more realistic situation, where scaling describes the $M(H)$ loops well over some extensive, but finite, range of field and temperature.

1. Scaling of $J(B)$ with respect to E at constant T

We have shown that by normalizing the current density and field scales by the peak position $(J_{\max},B_{\max})$ the measured magnetization loops trace out a universal function φ,

$$\frac{J}{J_{\max}(E,T)}=\varphi\left[\frac{B}{B_{\max}(E,T)}\right],$$

which in logarithmic coordinates becomes

$$\ln J-\ln J_{\max}(E,T)=\Phi[\ln B-\ln B_{\max}(E,T)] . \quad (2)$$

The formulation of Eq. (2) is slightly arbitrary because any characteristic feature (not just the fishtail peak) could be used to scale the curves, and hence the function Φ is not uniquely defined (Φ defines a set of functions which may be mapped onto each other by linear translations in logarithmic space). The electric field scaling can be expressed in a more general way by differentiating Eq. (2) with respect to $\ln E$ at constant B:

$$\left[\frac{\partial \ln J}{\partial \ln E}\right]_{B,T}=\left[\frac{\partial \ln B_{\max}}{\partial \ln E}\right]_T\left[\left[\frac{\partial \ln J_{\max}}{\partial \ln B_{\max}}\right]_T-\Phi'\right] . \quad (3)$$

The quantity $\Phi'=(\partial \ln J/\partial \ln B)_{E,T}$ will play an important role in what follows and has a direct physical interpretation as the (logarithmic) slope of the measured $M(H)$ loops. We will denote it as $\chi_{\ln}$ and call it the logarithmic susceptibility. Note that the ambiguity mentioned above is no longer present in Eq. (3) because $J_{\max}$ and $B_{\max}$ can be freely replaced by any other characteristic position $(J_{\text{char}},B_{\text{char}})$ on the loops, and scaling requires that

$$\left[\frac{\partial \ln J_{\max}}{\partial \ln B_{\max}}\right]_T=\left[\frac{\partial \ln J_{\text{char}}}{\partial \ln B_{\text{char}}}\right]_T=k_E(E,T) \quad (4)$$

and

$$\left[\frac{\partial \ln B_{\max}}{\partial \ln E}\right]_T=\left[\frac{\partial \ln B_{\text{char}}}{\partial \ln E}\right]_T=\gamma_E(E,T) . \quad (5)$$

The parameter $k_E(E,T)$ is the gradient of translations associated with changes in the electric field (see Fig. 2), and $\gamma_E(E,T)$ quantifies the electric field dependence of these translations.

Hence Eq. (3) can be written

$$S(B,E,T)=\gamma_E(E,T)[k_B(E,T)-\chi_{\ln}(B,E,T)] , \quad (6)$$

so that the scaling is uniquely described by a linear relationship between the normalized creep rate and the logarithmic susceptibility. Its behavior is quantified by the two scaling parameters $k_E(E,T)$ and $\gamma_E(E,T)$ which, for ideal scaling, do not depend on B.

To see the influence of the scaling, we can compare the magnetic field dependences of the measured creep rate $S(B)$ and the logarithmic susceptibility $\chi_{\ln}(B)$. Figure 4 shows that there is indeed a strong correlation between the forms of the two functions and that both have a close-to-linear B dependence over most of the field range.

The values of k_E and γ_E could be obtained from the dependence of the fishtail peak position on E using Eqs. (4) and (5), but a more general method (which does not require the presence of a fishtail peak and is also more informative because it includes data from the entire field range with equal weight) is to plot $S(B)$ versus $\chi_{\ln}(B)$, as shown in Fig. 5. In the higher-field region, these plots can be fitted by straight lines, as suggested by Eq. (6); the lines have gradient and intercept on the abscissa equal to $-\gamma_E$ and k_E, respectively. We will return to the low-field data in Sec. IV B 1.

Figure 6(a) shows γ_E and k_E as a function of temperature in the range $30<T<77$ K (the present approach becomes inapplicable at low temperatures for reasons that will be explained in Sec. IV B 2). Over this range $k_E=1.05\pm0.05$ and shows no systematic temperature dependence; $\gamma_E\approx0.04$ and tends to increase slowly with temperature.

2. Scaling with respect to T at constant E

The approach to quantifying the temperature scaling is essentially identical to the electric field case. We introduce two parameters γ_T and k_T, which are entirely analogous to γ_E and k_E, and so we have [see Eq. (6)]

$$\left[\frac{\partial \ln J}{\partial \ln T}\right]_{B,E}=\gamma_T(E,T)[k_T(E,T)-\chi_{\ln}(B,E,T)] , \quad (7)$$

with

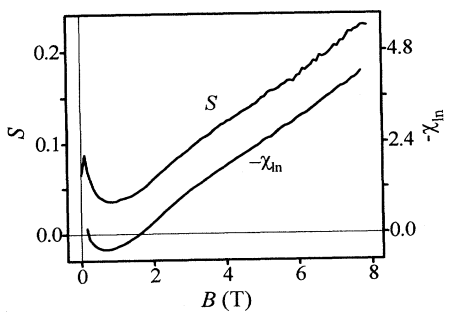

FIG. 4. Logarithmic susceptibility $\chi_{\ln}(B)$ and the creep rate $S(B)$ calculated, respectively, from the measured $J(B)$ at 50 K and its sweep rate dependence.

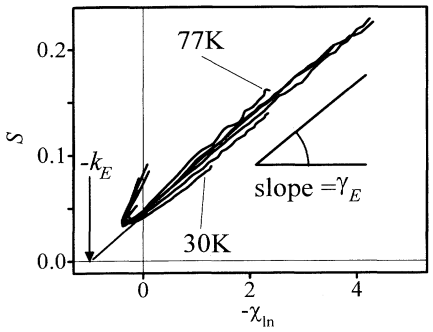

FIG. 5. $S(B)$ plotted against $\chi_{ln}(B)$ with B as the implicit variable for a series of temperatures between 30 and 77 K; the fishtail peak occurs at $\chi_{ln}(B)=0$. The steeper short segments correspond to low H, where self-field effects are significant. At each temperature, the higher-field data are almost linear; a straight-line fit to them has gradient $\gamma_E(T)$ and intercept on the abscissa equal to $-k_E(T)$.

$$k_T(T)=\left[\frac{\partial \ln J_{max}(T)}{\partial \ln B_{max}(T)}\right]_E \tag{8}$$

and

$$\gamma_T(T)=\left[\frac{B\ln B_{max}(T)}{\partial \ln T}\right]_E . \tag{9}$$

Again, it is implicit in ideal scaling that these parameters be B independent. In order to evaluate them, we could proceed as before by plotting $\partial \ln J/\partial \ln T$ versus χ_{ln}. However, it turns out to be more convenient to use the fishtail peak coordinates $J_{max}(T)$ and $B_{max}(T)$, and find $k_T(T)$ and $\gamma_T(T)$ directly from Eqs. (8) and (9), using the differences between magnetization loops at adjacent points.

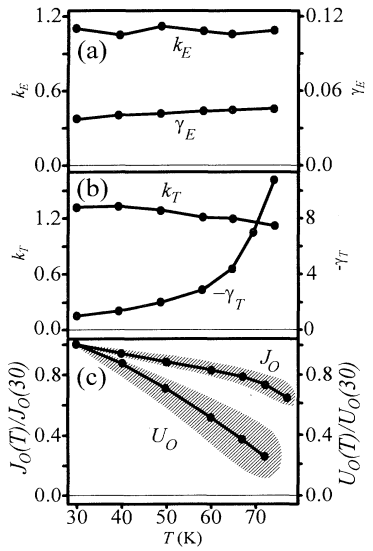

FIG. 6. Temperature dependence of the derived parameters: (a) $\gamma_E(T)$ and $k_E(T)$, as obtained from the linear fits of Fig. 5; (b) $\gamma_(T)$ and $k_T(T)$, as obtained from the temperature dependence of the coordinates of the fishtail peak [Eqs. (8) and (9)]; (c) The scale current density $J_0(T)$ and the scale energy $U_0(T)$, normalized to their values at 30 K and obtained from Eqs. (17) and (18). Estimated uncertainties are indicated by hatched areas.

For the illustrative sample used here, this procedure results in the dependences shown in Fig. 6(b); the value of k_T is very close to that of k_E, which is just a formal way of expressing the scaling equivalence of changes in E and T for this crystal (Sec. III, Fig. 2). On the other hand, γ_T does not have any direct connection to γ_E, lying in the range $-1>\gamma_T>-10$ and having a strong temperature dependence.

B. Realistic scaling

Scaling implies some systematic behavior of the vortex dynamics, and it would be unrealistic to expect a single model to describe the vortices at all fields and temperatures. The empirical observation is that scaling works over a substantial range of these variables, and the argument of this paper is that a single model might be expected to be valid over the same range. Elsewhere on the B-T plane, there might be a different scaling or no scaling at all.

1. *Different vortex regimes*

Deviations from scaling are evident in the low-field magnetization data as presented in Fig. 3, and they show up in Fig. 5 as the steeper, short segments at negative $\chi_{ln}(B)$ (as was pointed out in Sec. IV A 1, the latter representation is general and does not depend upon the presence of a fishtail peak). At higher fields and for a wide range of temperatures, the plots of $S(B)$ against $\chi_{ln}(B)$ are indeed linear within the experimental noise, and that is the appropriate criterion of whether there is significant scaling over a substantial sector of the B-T plane. We may then infer that within that sector a single model of vortex behavior should be dominant. The analysis then proceeds as described for ideal scaling, and the data can be used to extract the fundamental vortex parameters, as will be described in Sec. V.

The low-field behavior is complicated by self-field effects,[10] and is more evident in the well-oxygenated crystals described in Ref. 6. There we concluded that the low- and high-field regimes (denoted region 1 and region 2) are associated with distinct vortex dynamics; in our recent systematic study of deoxygenated crystals,[9] we find that as oxygen is removed, region 1 shrinks on the B-T plane and region 2 expands.

2. *Low temperatures*

At temperatures below about 40 K in well-oxygenated $YBa_2Cu_3O_{7-\delta}$ and at correspondingly lower temperatures in deoxygenated crystals, J becomes only weakly dependent on B (apart from the low-field region) up to the maximum fields available in magnetometers, typically 10 T. Also, S hardly varies from its "universal value" of 0.03.[13] The measured $S(B)$ and $\chi_{ln}(B)$ then shrink to a

small cluster of points when plotted in the form of Fig. 5, so that straight-line fits to obtain γ_E and k_E are impossible and our procedure becomes inapplicable. It is for that reason that we do not show data here below about 30 K.

This inability to extract useful parameters at low temperatures is not because the approach is flawed, but rather reflects the experimental limitations. As we have pointed out previously,[10] information about $U_{\rm eff}$ is contained within the *second* derivatives of the E-J-B surface, and if the derivatives $S(B)$ and $\chi_{\rm ln}(B)$ are nearly constant over the experimental range of B, there is little that can be learned about the vortex dynamics.

V. IMPLICATIONS OF SCALING FOR FLUX CREEP

A. Rate equation and the E-J-B surface

We now consider the physical significance of the experimentally observed scaling and the four parameters k_E, γ_E, k_T, and γ_T obtained from it. We emphasize that so far we have made no assumptions or utilized any model for the vortex behavior, so that without any circularity of the argument we can now analyze the implications of scaling for the vortex dynamics of the system.

The usual description of flux creep is given by the rate equation[8,14] in terms of thermally activated motion of vortices and can be written as

$$E = B\omega d \exp\left[\frac{-U_{\rm eff}(J,B,T)}{kT}\right], \tag{10}$$

where ω is a characteristic attempt frequency, d is a characteristic hop distance, and $U_{\rm eff}(J,B,T)$ is the potential energy barrier in the presence of a driving force proportional to J and B. The physics of the system is contained primarily within the $U_{\rm eff}(J,B,T)$ function.

It is worthwhile emphasizing that when a sample is taken round an isothermal magnetization loop with fixed magnetic field sweep rate, H' and therefore E are constant, and so (apart from a slow logarithmic dependence on B) $U_{\rm eff}$ is being held constant. This is achieved by the dependences of $U_{\rm eff}$ on J and on B exactly counterbalancing each other.

Isothermal magnetic measurements are conveniently described by a three-dimensional E-J-B surface,[10] and we utilize the geometric relation

$$\left[\frac{\partial \ln E}{\partial \ln J}\right]_B \left[\frac{\partial \ln J}{\partial \ln B}\right]_E \left[\frac{\partial \ln B}{\partial \ln E}\right]_J = -1 .$$

Recalling that $S = (\partial \ln J/\partial \ln E)_B$, the susceptibility $\chi_{\rm ln}$ is

$$\chi_{\rm ln} = \left[\frac{\partial \ln J}{\partial \ln B}\right]_{E,T} = -S\left[1 - \frac{1}{kT}\left[\frac{\partial U_{\rm eff}}{\partial \ln B}\right]_{J,T}\right] .$$

Therefore it is evident immediately that a relationship between S and $\chi_{\rm ln}$, such as that shown in Fig. 5, bears directly on the B dependence of $U_{\rm eff}$.

B. Characteristic energy U_0 and characteristic current density J_0

In order to progress further we need to suggest a functional form for $U_{\rm eff}$ while retaining as much generality as possible. Following Schnack *et al.*,[8] we separate $U_{\rm eff}(J,B,T)$ into an energy term and a current density term:

$$U_{\rm eff}(J,B,T) = U_0(B,T)\, V\left[\frac{J}{J_0(B,T)}\right], \tag{11}$$

where $U_0(B,T)$ is a characteristic energy barrier and $J_0(B,T)$ is a characteristic current density (or equivalently a force density). The function $V(J/J_0)$ describes the influence of the driving force on the effective activation energy $U_{\rm eff}$. Clearly, the absolute magnitudes of $U_0(B,T)$, $V(J/J_0)$, and $J_0(B,T)$ are undefined within multiplicative factors.

We allow both U_0 and J_0 to be functions of B and T, and the purpose of the present analysis is to see how much can be learned about their form from experiment. We proceed by combining Eqs. (10) and (11):

$$\ln\left[\frac{vB}{E}\right] = \frac{U_0(B,T)}{kT} V\left[\frac{J}{J_0(B,T)}\right], \tag{12}$$

where v is the velocity ωd. We have measured the number $\ln(vB/E)$ to be 25 ± 5 at 20 K (see Appendix B), and so it is large compared to unity and therefore insensitive to changes in v. Hence we may neglect any field or temperature dependence of v in the following analysis (any influence that these small dependences may have will become incorporated in the functions U_0 and J_0).

As shown in Appendix A, differentiation of Eq. (12) with respect to each of $\ln B$, $\ln E$, and $\ln T$ yields equations of just the same form as Eqs. (6) and (7), and so results in straightforward expressions for k_E, γ_E, k_T, and γ_T:

$$k_E = \left[\frac{\partial \ln J_0}{\partial \ln B}\right]_T , \tag{13}$$

$$\gamma_E = \left[1 - \ln\left[\frac{vB}{E}\right]\left[\frac{\partial \ln U_0}{\partial \ln B}\right]_T\right]^{-1} , \tag{14}$$

$$k_T = k_E + \frac{1}{\gamma_T}\left[\frac{\partial \ln J_0}{\partial \ln T}\right]_B , \tag{15}$$

$$\gamma_T = -\gamma_E \ln\left[\frac{vB}{E}\right]\left[1 - \left[\frac{\partial \ln U_0}{\partial \ln T}\right]_B\right] . \tag{16}$$

These results show that the experimentally observed scaling described in Sec. III can be translated *directly* into the field and temperature dependences of U_0 and J_0 through the four measured scaling parameters k_E, γ_E, k_T, and γ_T. It is the simplicity of this linkage, requiring neither complex manipulation of the experimental data nor a model for the vortex dynamics and resting solely on the rather general form for $U_{\rm eff}$ of Eq. (11), that makes it so significant.

VI. EVALUATION OF THE FIELD AND TEMPERATURE DEPENDENCES OF U_0 and J_0

A. Temperature dependence of $U_0(B,T)$ and $J_0(B,T)$

Equation (15) shows that the temperature dependence of J_0 is simply proportional to the difference between $M(H)$ loop scaling with respect to temperature and with respect to electric field, as expressed by the parameters k_T and k_E. It can be assessed immediately from a plot of the measured data, as in Fig. 2, which shows that for the illustrative sample these parameters are very nearly equal (Fig. 6).

We integrate Eqs. (15) and (16) to find $J_0(T)$ and $U_0(T)$ explicitly:

$$J_0(T)=J(T_0)\exp\left[\int_{T_0}^{T}\gamma_T(k_T-k_E)\frac{dT}{T}\right], \tag{17}$$

$$U_0(T)=U_0(T_0)\exp\left[\int_{T_0}^{T}\left[1+\frac{\gamma_T}{\ln(vB/E)\gamma_E}\right]\frac{dT}{T}\right]. \tag{18}$$

Figure 6(c) displays the results for the specific $TmBa_2Cu_3O_{6.8}$ crystal and the near constancy of $J_0(T)$ with temperature.

B. Field dependences of $J_0(B,T)$ and $U_0(B,T)$

Recalling that scaling of the $M(H)$ loops requires k_E and γ_E to be independent of B (Sec. IV), we can see from Eqs. (13) and (14) that $J_0(B)$ and $U_0(B)$ must have power law dependences. We have

$$J_0(B,T)=\Lambda(T)B^{k_E}$$

and

$$U_0(B,T)=\Psi(T)B^{(\gamma_E-1)/\gamma_E\ln(vB/E)},$$

where $\Lambda(T)$ and $\Psi(T)$ describe the temperature dependences of $J_0(B,T)$ and $U_0(B,T)$, respectively.

The experimental values for our illustrative sample as given in Sec. III and Fig. 6(a) yield

$$J_0(B,T)=\Lambda(T)B^{1.05\pm0.05}$$

and [with $\ln(vB/e)=25\pm5$ as evaluated in Appendix B]

$$U_0(B,T)=\Psi(T)B^{-1.0\pm0.3},$$

without any significant temperature dependence of the exponents; hence, the B and T dependences are separable. Thus, within experimental uncertainties, we have for this $TmBa_2Cu_3O_{6.8}$ crystal simply $J_0(B)\propto B$ and $U_0(B)\propto 1/B$.

We can now understand the presence of the fishtail peak in terms of the field dependences of $J_0(B,T)$ and $U_0(B,T)$: At low fields, $U_{\rm eff}$, and so also the measured current density $J(B,T)$, is dominated by the increase of $J_0(B,T)$ with field, but eventually it is overtaken by the decrease in $U_0(B,T)$ (Fig. 7).

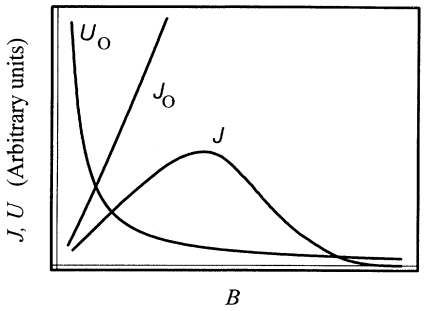

FIG. 7. Schematic field dependences of the parameters $U_0(B)$ and $J_0(B)$ and the resultant current density $J(B)$, showing how the fishtail peak in the magnetization arises from the interplay of the two parameters.

C. $U_{\rm eff}(J)$ function

Knowledge of $J_0(B)$ and $U_0(B)$ allows us to infer the form of $V(J)$ or, equivalently, $U_{\rm eff}(J)$. As we have just seen, simple power laws $J_0=\Lambda(T)B$ and $U_0=\Psi(T)/B$ fit the data for the $TmBa_2Cu_3O_{6.8}$ crystal rather well. From Eq. (12) we then have

$$BT=\frac{\Psi(T)}{\ln(vB/E)k}V\left[\frac{J(B,T)}{\Lambda(T)B}\right], \tag{19}$$

and it is natural to plot BT as a function $J(B)/B$. These data fit to a logarithmic form for $V(J)$ (Fig. 8), giving

$$J(B,T)=\Lambda(T)B\exp\left[-\frac{kTB}{\Psi(T)}\ln\left[\frac{vB}{E}\right]\right]. \tag{20}$$

The creep rate S can be obtained immediately from this simple fit:

$$S(B,T)=\frac{kT}{\Psi(T)}B, \tag{21}$$

which is, of course, consistent with the observed linear dependence of S on B shown above the low-field region in Fig. 4.

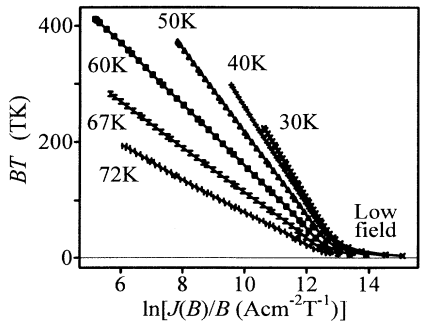

FIG. 8. Isotherms of experimental data plotted in the form BT against $\ln[J(B)/B]$. In the low-field region, self-field effects may be significant. The higher-field data fit well to straight lines, suggesting that the function $V(J)$, which controls the current dependence of $U_{\rm eff}$, is well approximated by a simple logarithm (Sec. VI C).

VII. COMPARISON TO THEORY

The thrust of the present paper is to show how key parameters can be extracted reliably from magnetization data. The meeting point with theory is the comparison with the predicted dependences of $U_{\rm eff}$ on J, B, and T. We make this comparison to illustrate that theoretical models often yield characteristic critical currents J_c and energy barriers U_c, and that the temperature and field dependences of these should relate to the scaling parameters of Eqs. (13)–(16). However, as the absolute values of U_0 and J_0 are not uniquely defined, direct associations between U_c and U_0 or J_c and J_0 must be treated with caution.

It is not appropriate here to review exhaustively the theoretical situation,[15] but to illustrate the way forward, we make a brief comparison of our results with the original theory of collective pinning as proposed by Larkin and Ovchinnikov.[16] The presence of random disorder causes the vortex lattice to be replaced by a glassy array, in which the vortex positions are correlated only within a flux bundle of volume Ω_c. The pinning forces in the volume Ω_c add randomly, so that $U_c \propto F_c \propto \Omega_c^{1/2}$, where U_c is the energy with which the bundle is pinned and F_c is the maximum pinning force on the bundle. Given that the pinning force per unit volume is $J_c B$, we have $J_c B = F_c/\Omega_c = \Omega_c^{-1/2}$; hence, $U_c \propto 1/(J_c B)$. If $U_c(B)$ and $J_c(B)$ have power law dependences $U_c \propto B^u$ and $J_c \propto B^j$, we obtain $(u+j)=-1$. Note that this result is independent of the field dependence of Ω_c, which is a complicated issue.

We can make a direct comparison to the experimental results as follows. For the illustrative $TmBa_2Cu_3O_{6.8}$ crystal, we have measured $J_0(B) \propto B$ and $U_0(B) \propto B^{-1}$, which implies $J_c(B) \propto B$ and $U_c(B) \propto B^{-1}$ and hence $(u+j)=0(\pm 0.3)$, in contradiction with the Larkin-Ovchinnikov result.

The collective pinning theory has been modified to account for sample anisotropy and harmonic thermal fluctuations of the vortex lattice.[15,17] In this rather complicated picture, several different pinning regimes are predicted. All but one predict a decreasing J_c with field and hence disagree entirely with our results; the one exception is when nonlocal effects soften the vortex lattice and result in $J_c \propto B^{0.75}$ and $U_c = \text{const}$. This is a somewhat better description of our $TmBa_2Cu_3O_{6.8}$ data, but certainly not satisfactory. Also, the inferred logarithmic dependence of $U_{\rm eff}$ on J (Sec. VI C) is not predicted by this theory, but has been observed in other experiments.[18]

Stronger evidence about the vortex dynamics can be obtained from a comparative study of several crystals[6] and particularly from the behavior as the anisotropy is altered by withdrawing oxygen.[9] Different regimes certainly are visible, and they can be quantified by applying the systematic procedure for analyzing the experimental data developed here.

VIII. CONCLUSIONS

The data from magnetization experiments contain all the information relevant to vortex dynamics in superconductors, but previous analyses have been rather complicated and so obscured the connection between the field and temperature dependences of M and S on the one hand and key pinning parameters on the other.

Here we have developed an analytical procedure that incorporates the commonly observed scaling behavior of the $M(H)$ loops in $(R)Ba_2Cu_3O_{7-\delta}$ and shown that it yields quantities that can be related in a rather simple fashion to the usual description of thermally activated vortex motion. The important parameters that measure the temperature and field dependences of the characteristic current density and energy scales can then be obtained directly, and so much more transparently, from the experimental data, without any deconvolution or fitting parameters. All of this can be accomplished without introducing any specific model for the vortex dynamics.

Deliberately, in this paper we have chosen for simplicity to illustrate the value of the procedure by applying it to the magnetization data obtained from just one $TmBa_2Cu_3O_{7-\delta}$ crystal. The manner in which the characteristic energy and current scales change with oxygen concentration will be discussed elsewhere.[9]

ACKNOWLEDGMENTS

Financial support for this research has been provided by the Engineering and Physical Sciences Research Council, the Royal Society and by NATO Linkage Grant No. HT 931241.

APPENDIX A: DERIVATION OF THE SCALING PARAMETERS FROM THE RATE EQUATION

We start with Eq. (11),

$$\ln\left[\frac{vB}{E}\right]=\frac{U_0}{kT}\,V\left[\frac{J}{J_0}\right]. \tag{A1}$$

Differentiating (A1), with respect to $\ln B$, yields

$$1=\ln\left[\frac{vB}{E}\right]\left[\frac{\partial \ln U_0}{\partial \ln B}\right]_T + \frac{U_0}{kT}\frac{J}{J_0}V'\left[\left[\frac{\partial \ln J}{\partial \ln B}\right]_{E,T}-\left[\frac{\partial \ln J_0}{\partial \ln B}\right]_{E,T}\right], \tag{A2}$$

with respect to $\ln E$,

$$1=-\frac{U_0}{kT}\frac{J}{J_0}V'\left[\frac{\partial \ln J}{\partial \ln E}\right]_{B,T}, \tag{A3}$$

and, with respect to $\ln T$,

$$0=\ln\left[\frac{vB}{E}\right]\left[1-\left[\frac{\partial \ln U_0}{\partial \ln T}\right]_B\right] - \frac{U_0}{kT}\frac{J}{J_0}V'\left[\left[\frac{\partial \ln J}{\partial \ln T}\right]_{B,E}-\left[\frac{\partial \ln J_0}{\partial \ln T}\right]_B\right]. \tag{A4}$$

Substitution of (A3) into (A2) gives

$$\left[\frac{\partial \ln J}{\partial \ln E}\right]_{B,T}=\frac{(\partial \ln J_0/\partial \ln B)_T-(\partial \ln J/\partial \ln B)_{E,T}}{1-\ln(vB/E)(\partial \ln U_0/\partial \ln B)_T}. \tag{A5}$$

A comparison of (A5) with (5) shows that

$$k_E = \left[\frac{\partial \ln J_0}{\partial \ln B}\right]_T \tag{A6}$$

and

$$\gamma_E = \left[1 - \ln\left[\frac{vB}{E}\right]\left[\frac{\partial \ln U_0}{\partial \ln B}\right]_T\right]^{-1} . \tag{A7}$$

Substitution (A2) in (A4) gives

$$\left[\frac{\partial \ln J}{\partial \ln T}\right]_{B,E} = -\frac{\ln(vB/E)[1-(\partial \ln U_0/\partial \ln T)_B]}{1-\ln(vB/E)(\partial \ln U_0/\partial \ln B)_T} \times \left[\left[\frac{\partial \ln J_0}{\partial \ln B}\right]_T - \left[\frac{\partial \ln J}{\partial \ln B}\right]_{E,T}\right] + \left[\frac{\partial \ln J_0}{\partial \ln T}\right]_B . \tag{A8}$$

A comparison of (A8) with (6) shows that

$$k_T = k_E + \frac{1}{\gamma_T}\left[\frac{\partial \ln U_0}{\partial \ln T}\right]_B \tag{A9}$$

and

$$\gamma_T = -\gamma_E \ln\left[\frac{vB}{E}\right]\left[1 - \left[\frac{\partial \ln U_0}{\partial \ln T}\right]_B\right] . \tag{A10}$$

Equations (A6), (A7), (A9), and (A10) are the key results that are used in the analysis. Note that no approximations have been used; for example, we have *not* assumed that there is simple power law behavior of E on J.

APPENDIX B: EVALUATION OF $\ln(vB/E)$

From Eq. (A10),

$$\ln\left[\frac{vB}{E}\right] = -\frac{\gamma_T/\gamma_E}{(1-\partial \ln U_0/\partial \ln T)_B} .$$

At low temperatures U_0 can be considered to be insensitive to temperature[8,14] and hence

$$\ln\left[\frac{vB}{E}\right] = -\frac{\gamma_T}{\gamma_E} .$$

Measurements of γ_E and γ_T between 30 and 80 K allow extrapolation to $T=0$; for the present sample, we find $\ln(vB/E)=25\pm5$.

[1] L. Civale, M. W. McElfresh, A. D. Marwhich, F. Holtzberg, and C. Field, Phys. Rev. B **43**, 1373 (1991).

[2] K. A. Delin *et al.*, Phys. Rev. B **46**, 11 092 (1992).

[3] A. A. Zhukov, H. Kupfer, S. A. Klestov, V. I. Voronkova, and V. K. Yanovskey, J. Alloys Compounds **195**, 479 (1993).

[4] M. Oussena, P. A. J. de Groot, A. Marshall, and J. S. Abell, Phys. Rev. B **49**, 1484 (1994).

[5] L. Klein, E. R. Yacoby, Y. Yeshurun, A. Erb, G. Muller-Vogt, V. Breit, and H. Wuhl, Phys. Rev. B **49**, 4403 (1994).

[6] L. F. Cohen, A. A. Zhukov, G. K. Perkins, H. J. Jensen, S. A. Kestlov, V. Voronkova, S. Abell, H. Kupfer, T. Wolf, and A. D. Caplin, Physica C **230**, 1 (1994).

[7] A. A. Zhukov, L. F. Cohen, G. K. Perkins, A. D. Caplin, S. A. Klestov, V. I. Voronkova, A. Marshall, and S. Abell, Physica B **194-196**, 1921 (1994).

[8] H. G. Schnack, R. Griessen, J. G. Lensink, and Wein Hai-Hu, Phys. Rev. B **48**, 13 178 (1993).

[9] G. K. Perkins *et al.* (unpublished).

[10] A. D. Caplin, L. F. Cohen, G. K. Perkins, and A. A. Zhukov, Supercond. Sci. Technol. **7**, 412 (1994).

[11] C. P. Bean, Rev. Mod. Phys. **36**, 31 (1964).

[12] L. Pust, Supercond. Sci. Technol. **3**, 598 (1990).

[13] A. P. Malozemoff and P. A. Fisher, Phys. Rev. B **42**, 6784 (1990).

[14] M. P. Maley, J. O. Willis, H. Lessure, and M. E. Mchenry, Phys. Rev. B **42**, 2639 (1990).

[15] G. Blatter, M. V. Feigel'man, V. B. Geshkenbein, A. I. Larkin, and V. M. Vinokur, Rev. Mod. Phys. (to be published).

[16] A. I. Larkin and Yu. N. Ovchinnikov, J. Low Temp. Phys. **34**, 409 (1979).

[17] M. V. Feigel'man and V. M. Vinokur, Phys. Rev. B **41**, 8986 (1990).

[18] E. Zeldov, N. M. Amer, G. Koren, A. Gupta, M. W. McElfresh, and R. J. Gambino, Appl. Phys. Lett. **56**, 680 (1990).